JOURNAL OF THERMOPHYSICS AND HEAT TRANSFER
Vol. 22, No. 1, January–March 2008

Experimental and Numerical Studies of Thermally Induced Acoustic Waves in an Enclosure

Yiqiang Lin* and Bakhtier Farouk†
Drexel University, Philadelphia, Pennsylvania 19104

DOI: 10.2514/1.29776

The behaviors of thermally induced acoustic waves generated by the rapid heating of a bounding solid wall in a closed cylindrical tube are investigated experimentally. The induced flow and pressure fields due to rapid heating are also numerically simulated. In the experiments, a resistance–capacitance circuit is used to generate a rapid temperature increase in a thin nickel foil located at one end of the closed cylindrical tube. The thermally generated pressure (acoustic) waves undergo repeated reflections at the two ends of the tube and gradually decay. The time-dependent pressure variation in the tube and the voltage and temperature histories at the foil are recorded by a fast-response measurement system. The characteristics of the generation, propagation, and decay of the acoustic waves are measured by two different transducers (Brüel & Kjær model 4193 and Endevco model 8507C-1). To simulate the experiments numerically, the compressible unsteady axisymmetric Navier–Stokes equations are solved by a highly accurate algorithm. Both the experimental and numerical studies predict similar pressure wave shapes and profiles. The measured decay rate of the acoustic waves is found to be somewhat faster than the numerically predicted rate.

Nomenclature

A	=	area of the foil
a	=	acoustic speed
C	=	capacitance
c	=	heat capacitance of the foil
E	=	total energy
e	=	internal energy
g	=	gravitational acceleration
k	=	thermal conductivity
L	=	length of the cylinder
M	=	Mach number
p	=	pressure
R	=	specific gas constant
r	=	radial coordinate
T	=	temperature
t	=	time
V	=	voltage
z	=	axial coordinate
δ	=	thickness of the foil
θ	=	angular coordinate
μ	=	dynamic viscosity
ρ	=	density

Subscripts

f	=	foil
n	=	normal to the wall
w	=	wall position
0	=	initial

I. Introduction

WHEN a compressible fluid within an enclosure is subjected to a rapid temperature increase along a confining wall, the fluid in the immediate vicinity of the wall expands, resulting in a fast increase in the local pressure in the vicinity of the heated surface. The rapid heating leads to the production of pressure waves, which propagate at nearly the local sound speed [1]. These thermally induced acoustic waves are repeatedly reflected from the chamber walls and a flowfield may eventually be developed within the enclosure. This flow can cause unwanted disturbances in otherwise static processes such as cryogenic storage or may introduce a convective heat-transfer mode to the systems in zero-gravity environments, in which conduction and radiation are the only heat-transfer modes. In near-critical fluids, characterized by low heat diffusivity, the thermally induced acoustic convection mode of heat transport can become important, especially in a reduced-gravity environment [2].

The problem of thermally induced acoustic waves in a quiescent semi-infinite body of a perfect gas subjected to a step change in temperature at the solid wall has been studied analytically [3–5] to determine how the sound intensity depends on the history of the wall temperature. Ozoe et al. [6,7] obtained their solutions by employing the upwind scheme to solve the governing equations, and as a consequence, the results showed effects of substantial numerical diffusion. Brown and Churchill [8] also showed that rapid heating of a solid surface bounding a region of gas generates a slightly supersonic wave with positive amplitude in pressure, temperature, density, and mass velocity. Using a high-order numerical scheme, Farouk et al. [9] predicted the early time behavior of thermally induced acoustic waves in a compressible-fluid-filled cavity. Aktas and Farouk [10] studied the interaction of thermally induced acoustic waves and buoyancy-induced flows in an enclosure that is rapidly heated on one side. More recently, Lin et al. [11] numerically investigated the effect of gravity on flows generated by thermally induced acoustic waves in an enclosure in which a side wall is nonuniformly heated.

The generation of thermoacoustic waves in gases has been studied experimentally by only a few investigators. Parang and Salah-Eddine [12] investigated the thermoacoustic convection phenomena in a cylinder containing air in normal and reduced-gravity environments. In their measurement, results for air temperature (no oscillations) were recorded due to the small oscillation amplitude and low sample rate of measurement, but the air temperatures were found to rise much faster than the computational results of pure conduction. No pressure measurements were reported by the preceding authors. Experimental measurements of pressure waves generated by rapid heating of a surface were first reported by Brown and Churchill [13]. In their experiments, the rapid heating process was achieved by a resistance–capacitance (R–C) circuit. The pressure measurements

Received 16 January 2007; accepted for publication 27 August 2007.

*Graduate Student, Department of Mechanical Engineering and Mechanics, 3141 Chestnut Street.

†Professor, Department of Mechanical Engineering and Mechanics, 3141 Chestnut Street. Senior Member AIAA.

clearly demonstrated the generation of acoustic waves by rapid heating of the wall.

In the present paper, we experimentally and numerically investigate the generation, propagation, and decay of thermally induced acoustic waves in a cylindrical tube. In our experiments, the rapid temperature rise of wall is realized by rapid electrical heating of a thin metal foil by an R–C electrical circuit following Brown and Churchill [13]. The present numerical results of the pressure and velocity fields induced by rapid heating of a sidewall are obtained by directly solving the time-dependent compressible Navier–Stokes equations for an axisymmetric enclosure in which one of the side walls is heated rapidly and then allowed to cool gradually.

II. Experimental Apparatus and Procedure

A. Test Rig

The realization of a rapid increase of a wall temperature is the critical point in the experimental design. The temperature increase rate does not only influence the character of thermally induced acoustic waves, but it also determines whether the wave generated can be detected by a sensor. With the knowledge gained from past work [13], we use a direct-current heating of a metal-foil-covered end piece of a plastic tube by means of an R–C circuit. A schematic of the experimental setup is shown in Fig. 1.

A plastic tube with an inside diameter of 38 mm and a length of 201 mm is used for studying the thermally generated acoustic waves. A nickel foil completely covers one end of the tube and is attached with a mica end piece. A similar mica plate is also used at the other end of the tube. These mica plates ensure rigid reflecting surfaces for the pressure waves. In addition, flexible ethylene propylene diene monomer rubber plates and thick plastic plates are added at the back of the mica plate and anchored with the tube to ensure a good seal for the tube. The foil is anchored by two long copper bars that serve as connection wires and supports for the foil. The cross-sectional dimensions of the copper bars are 70×70 mm. This minimizes the voltage drop through the copper bar and also guarantees that the electric current flows through the foil evenly.

A very thin nickel foil (thickness of 6.0 μm and electrical resistivity of $6.84 \times 10^{-8}\ \Omega \cdot \mathrm{m}$) is used in the present study for rapid heating of its surface. A silicon control rectifier (SCR) (Littelfuse model TO-218X) with a 2.5-μs triggering time is used to fully discharge the capacitor. This arrangement provides a rapid rise of the foil temperature for generating the acoustic waves in the surrounding gas along the tube. Some other advantages of the R–C heating system include good repeatability, easy control of heating rate, and maximum temperature increase. The details of the apparatus and circuit elements are listed in Table 1.

In the present experimental setup, the dimensions of the foil (attached around a circular mica end piece) are 42 mm $\times$ 50 mm $\times$ 6.0 μm. The electrical resistance of the foil is calculated to be 0.014 Ω. By carefully calculating every component in the R–C circuit, the circuit efficiency $\varepsilon = R_{\mathrm{foil}}/R_{\mathrm{total}}$ is found to be about 53%. Several capacitors rated at 18.0, 27.0, and 56.0 mF are used for the measurements. The circuit time constant $\tau_{RC} = R_{\mathrm{total}} \cdot C$ is hence 0.0005, 0.00071, and 0.0015 s for $C = 18.0$, 27.0, and 56.0 mF, respectively.

Two different types of pressure probe (see Fig. 2) are used to measure and monitor the thermally generated acoustic waves in the tube. A condenser microphone (12.7-mm Brüel & Kjær model 4193)

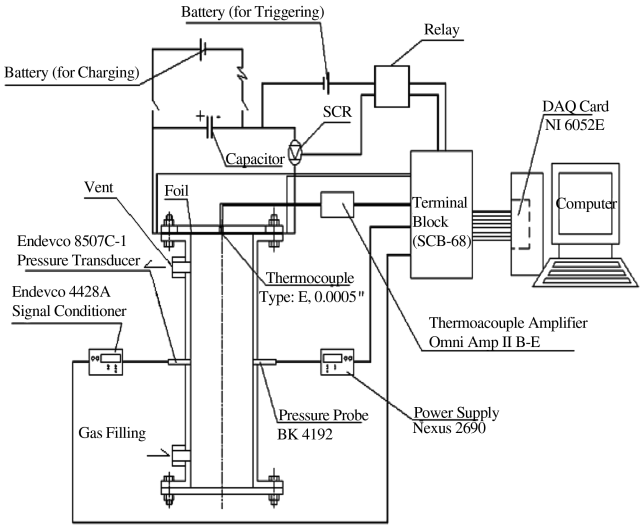

Fig. 1 Schematic of the experimental setup.

and a piezoresistive pressure transducer (Endevco model 8507C-1) are used. The probes are mounted transversely on the plastic tube (see Fig. 1), with the sensing surfaces flush with the tube inner wall. The probes are thus directly exposed to the gas and minimally interfere with the pressure wave propagation. The gaps between the probe boundaries and the holes are sealed by Dow Corning 832 noncorrosive sealant. The Brüel & Kjær condenser microphone is used because of its high sensitivity, fast response, and a wide frequency-response band. For the Brüel & Kjær condenser microphone, the detection system also includes a low-frequency adaptor (UC0211), a microphone preamplifier (model 2669), and a conditioning amplifier (ZN 2690). The piezoresistive pressure transducer Endevco 8507C-1 is used to measure the variation of the total pressure (sum of the static and dynamic components) in the tube. The Endevco 8507C-1 piezoresistive pressure transducer is powered and conditioned by a 4428A signal conditioner. The sensitivity of the Endevco transducer is not sufficient, however, to allow the measurement of the small dynamic-pressure fluctuations in the tube due to the sudden heating of the foil. Use of these two pressure transducers allows us to probe the thermally induced acoustic waves in greater detail than reported earlier.

The Brüel & Kjær 4193 condenser microphone (see Fig. 2a) consists of a metal housing. A delicate and highly tensioned diaphragm is placed ahead of a backplate. The distance between the diaphragm and the backplate changes if there is any pressure difference between the microphone housing and the tube volume exposed to the diaphragm. The corresponding capacitance variation is converted to a pressure signal by the microphone cartridge (not shown). To eliminate the influence of static-pressure variation and protect the diaphragm, the microphone housing is connected to the tube medium by a static-pressure equalization vent hole (Fig. 2a). The narrow vent hole ensures that the static pressure of the microphone housing follows the pressure variation in the tube. The vent hole is designed to equalize the static-pressure variations without suppressing the low-frequency components of the dynamic acoustic pressure that are to be measured. The time constant of the microphone's pressure equalization system is about 0.1 s; therefore,

Table 1 Specifications for the experimental system

No.	Part	Make and model	Specification
1	Capacitors	Sprague Antex A8	18, 27, and 56 mF
2	SCR	Littelfuse TO-218X	Max trigger time: 2.5 μs
3	Foil		Nickel: 0.006 mm thick, 99.95% resistivity, and $6.84 \times 10^{-8}\ \Omega \cdot \mathrm{m}$
4	Thermocouple	Omega Bare-8-E-12	12.7-mm-diam E type
5	Pressure probes	B&K 4193 with UC0211 adaptor	2 mV/Pa
		Endevco 8507C-1	2.1 mV/kPa
6	Data acquisition board	NI 6052E	333 kHz

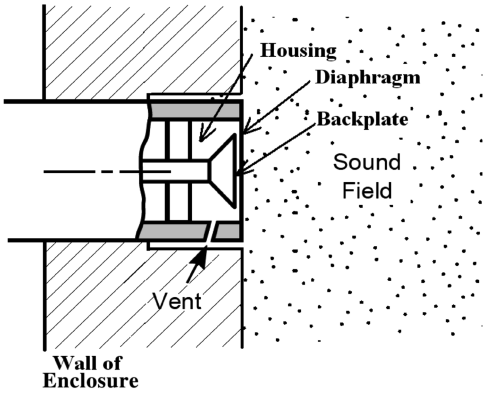

a) Brüel & Kjær microphone

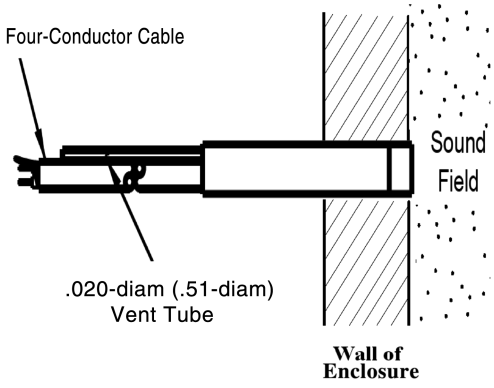

b) Endevco pressure transducer

Fig. 2 Details of the pressure probes.

the frequencies below 10 Hz are only affected by the vent hole. The Brüel & Kjær 4193 microphone is thus suitable for measuring the dynamic-pressure variation when the static pressure in the tube remains constant or varies slowly.

The Endevco 8507C-1 piezoresistive pressure transducer (shown in Fig. 2b), on the other hand, measures the variation of resistance due to the pressure difference between the two sides of the piezoresistive element. One side is exposed to the gas in the tube and the other side communicates with the outside ambient via a vent tube.

Other than the pressure measurements, the temperature and voltage drop histories of the foil (after the capacitor is discharged) are also recorded in our measurements. Previous numerical studies [10] of thermally generated acoustic waves by a rapidly heated surface show that the early temperature behavior of the heated surface (first several microseconds), has a significant influence on the behavior of the acoustic wave generated. Hence, we pay special attention to the measurement of the foil temperature at early times after the capacitor is discharged. Chromel–constantan type-E thermocouples with a diameter of 12.7 μm are used for their fast response time. The attachment of thermocouple on the foil is also critical. Silver adhesive (503, Electron Microscope Science) is used (chosen after evaluating many other brands of adhesives), mainly for its high thermal conductivity and ease of applicability. Because of its heat capacitance, the adhesive slows down the response time of the thermocouple at the very early time. The signals from the thermocouple probe are conditioned by an Omega Omni Amp IIB-E conditioning amplifier. The amplifier not only amplifies the weak signal from the thermocouple, but also isolates the high-frequency electrical disturbance by its interior signal-conditioning circuit. Although the amplifier eliminates the electrical disturbance at early time, it does not accurately record the peak value of the temperature rise of the foil (due to signal conditioning by the Omega Omni Amp IIB-E amplifier).

The analog temperature, pressure, and voltage measurements are recorded, digitized, and saved through a National Instruments SCB-68 terminal block and a 6052E data acquisition (DAQ) board. The high sample rate (333 kHz) of the 6052E DAQ board guarantees that the signals are recorded with high fidelity. The data acquisition system also provides a voltage output to a relay to control the triggering time of the SCR.

B. Experimental Method

Before each experiment, all devices are powered up and run such that the warm-up time requirements are met. All modules and devices are checked for the reliability of the experiment. The capacitor is charged up to a desired voltage V_0, which is measured by an HP 34401A multimeter. The LabView 7.0 software is used to record the signals of temperature, voltage, and pressure in the experiments and provide controlling signal. The SCR is triggered to initiate the experiment. The capacitor is discharged, causing rapid heating of the foil. The foil temperature gradually falls after the initial rapid rise. For most experiments, data are collected for about 5.1 s. After one experiment is carried out, the experimental conditions are initialized before the next set of measurements is made. Each experiment is repeated several times to confirm the measurements.

III. Numerical Method

The thermally induced acoustic waves are also numerically simulated. Because the heating foil used is thin and highly conductive, the spatial variation of the surface temperature of the foil is negligible. The flowfield inside the tube is thus considered to be two-dimensional (r and z). The schematic of the computational domain (19.0 × 201.0 mm) considered is shown in Fig. 3. Initially, the air in the chamber is considered as quiescent everywhere. At $t > 0$, the left wall temperature undergoes rapid increase and subsequent decay.

A. Mathematical Model

The generation and propagation of thermally induced acoustic waves are governed by the Navier–Stokes equations for a compressible fluid. In the two-dimensional cylindrical coordinates, these equations can be expressed in the conservative form as

$$\frac{\partial \rho}{\partial t} + \frac{1}{r}\frac{\partial (\rho r u_r)}{\partial r} + \frac{\partial (\rho u_z)}{\partial z} = 0 \tag{1}$$

$$\frac{\partial (\rho u_r)}{\partial t} + \frac{1}{r}\frac{\partial (r\rho u_r^2)}{\partial r} + \frac{\partial (\rho u_r u_z)}{\partial z} = -\frac{\partial p}{\partial r} + \rho f_r + \frac{1}{r}\frac{\partial (r\tau_{rr})}{\partial r} + \frac{\partial \tau_{rz}}{\partial z} - \frac{\tau_{\theta\theta}}{r} \tag{2}$$

$$\frac{\partial (\rho u_z)}{\partial t} + \frac{1}{r}\frac{\partial (r\rho u_r u_z)}{\partial r} + \frac{\partial (\rho u_z^2)}{\partial z} = -\frac{\partial p}{\partial z} + \rho f_z + \frac{1}{r}\frac{\partial (r\tau_{rz})}{\partial r} + \frac{\partial \tau_{zz}}{\partial z} \tag{3}$$

$$\frac{\partial E}{\partial t} + \frac{1}{r}\frac{\partial (ru_r E + ru_r p)}{\partial r} + \frac{\partial (u_z E + u_z p)}{\partial z} = \frac{1}{r}\frac{\partial (rq_r)}{\partial r} + \frac{\partial q_z}{\partial z} + \Phi + \rho \boldsymbol{f} \cdot \boldsymbol{V} \tag{4}$$

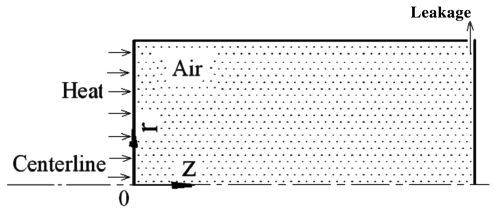

Fig. 3 Computational domain.

where the total energy $E = \rho([(V \cdot V)/2] + C_v T)$. The components of stress tensor τ are

$$\tau_{rr} = \mu' \left[\frac{1}{r} \frac{\partial (r u_r)}{\partial r} + \frac{\partial u_z}{\partial z} \right] + 2\mu \frac{\partial u_r}{\partial r} \tag{5}$$

$$\tau_{zz} = \mu' \left[\frac{1}{r} \frac{\partial (r u_r)}{\partial r} + \frac{\partial u_z}{\partial z} \right] + 2\mu \frac{\partial u_z}{\partial z} \tag{6}$$

$$\tau_{\theta\theta} = \mu' \left[\frac{1}{r} \frac{\partial (r u_r)}{\partial r} + \frac{\partial u_z}{\partial z} \right] + 2\mu \frac{u_r}{r} \tag{7}$$

$$\tau_{rz} = \tau_{zr} = \mu \left(\frac{\partial u_z}{\partial r} + \frac{\partial u_r}{\partial z} \right) \tag{8}$$

The components of the heat flux vector are written as

$$q_r = -k \frac{\partial T}{\partial r} \tag{9}$$

$$q_z = -k \frac{\partial T}{\partial z} \tag{10}$$

and the viscous dissipation term in Eq. (4) is given as

$$\Phi = \frac{\partial [(\tau_{rr} u_r + \tau_{rz} u_z) r]}{\partial r} + \frac{\partial [(\tau_{zr} u_r + \tau_{zz} u_z) r]}{\partial z} \tag{11}$$

In addition, an equation of state for perfect gas is used to relate the temperature to the other thermodynamic characteristics:

$$p = \rho P T \tag{12}$$

B. Numerical Scheme and Boundary Conditions

The governing equations (except for the diffusion terms) are discretized using a finite volume method based on the flux-corrected transport (FCT) algorithm [14]. The diffusion terms (the viscous term in the momentum equations and the conduction terms in the energy equation) are discretized using a second-order central-difference approach. FCT is a high-order, nonlinear, monotone, conservative, and positivity-preserving method designed to solve a general one-dimensional continuity equation with appropriate source terms. This scheme has fourth-order phase accuracy and is able to resolve steep gradients with minimum numerical diffusion. Further details of the FCT algorithm used here are documented by Boris et al. [14]. Time-step splitting is used to couple all of the representative physical effects, including the two-dimensional computational domain.

No-slip boundary conditions are used at all solid walls. In the present computational method, the treatment proposed by Poinsot and Lele [15] is followed for implementing the boundary conditions for the density. Along any solid wall, the density is calculated from

$$\left(\frac{\partial \rho}{\partial t} \right)_w + \frac{1}{a_w} \left(-\frac{\partial \rho}{\partial n} + \rho a_w \frac{\partial u_n}{\partial n} \right)_w = 0 \tag{13}$$

where the subscript w signifies the location of the wall, and n is the direction normal to the wall.

To simulate the presence of possible leakage in the experimental tube, part of the side boundary is also considered as open (as shown in Fig. 3) in some of the calculations. A 50×1000 ($r \times z$) grid size is used for all calculations because the problem is essentially one-dimensional (in the z direction) for the short time-scale considered. A very fine mesh in the axial direction, in addition to the use of an explicit time-marching scheme, allows us to capture the characteristics of the thermally induced acoustic waves. In the simulations, we provide the transient temperature history of the foil as the temperature boundary condition for the heated wall. Defining the transient temperature history of the foil is rather challenging. We use the experimental measurements of both voltage and temperature decay to develop the thermal boundary condition for the heated wall for the numerical simulations (details are provided in Sec. IV.C).

IV. Results and Discussions

A. Experimental Results

Approximately 100 experimental runs are carried out with the test rig using air at ambient conditions ($p_0 = 1$ atm and $T_0 = 299$ K). The nickel foil used for the rapid heating is 6.0 μm thick. Several capacitors rated at 18.0, 27.0, and 56.0 mF are used for the measurements. For a given capacitor, a number of different charging voltages V_0 are applied.

Figure 4 exhibits the transient voltage drop across the foil with $C = 27$ mF and $V_0 = 30$ V. The response shows a typical R–C circuit discharge behavior. The foil voltage reaches the peak value at about 0.00003 s and then it gradually decreases to zero by about 0.005 s. The foil voltage is about 37% of the peak value at approximately $t = 0.0011$ s. This is close to the calculated circuit time constant $\tau_{RC} = R_{\text{total}} \times C = 0.00071$ s for $C = 27$ mF.

The corresponding temperatures measured by the thermocouple are shown in Figs. 5a and 5b. At early time $t < 0.02$ s, the measured temperature rise rate is found to be much slower than the corresponding voltage discharge rate. The temperature rise in the foil depends on the heat gain and loss to the air. It is also noted that during the capacitor discharge period, the electromagnetic disturbance is high, and the thermocouple cannot respond during the initial discharge period (for $t < 0.005$ s, approximately).

1. Pressure Measurements with the Brüel & Kjær and the Endevco Probes

Figures 6a and 6b show the traces of the pressure wave measured by the Brüel & Kjær microphone under the following conditions: $C = 27$ mF and $V_0 = 30$ V. The probe records a local peak (Fig. 6a) when the acoustic wave sweeps past the probe diaphragm during its motion from the heated side to the unheated side. The next peak indicates the reflected acoustic wave that now travels from the unheated side to the heated side. During the first several acoustic cycles (Fig. 6a), the wave shape shows steep fronts with long tails, which is consistent with the previous studies [9]. Because of the viscous dissipation and energy losses, the characteristic of the acoustic wave profile (i.e., sharp peak and steep front) gradually disappear. The measured Mach number of the acoustic wave is about

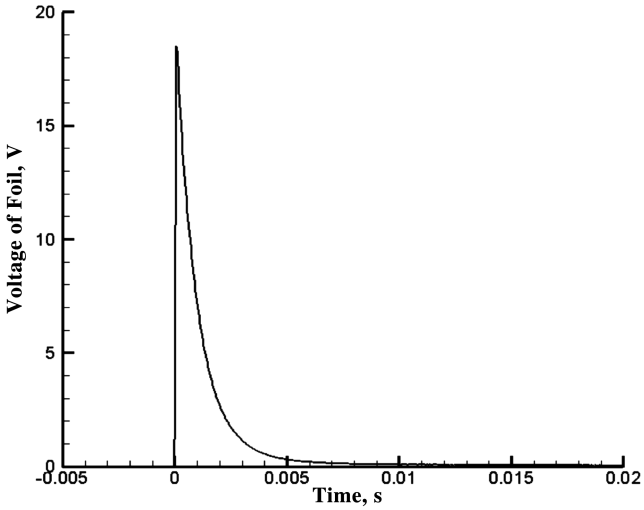

Fig. 4 Transient voltage drop across the foil; $C = 27$ mF and $V_0 = 30$ V.

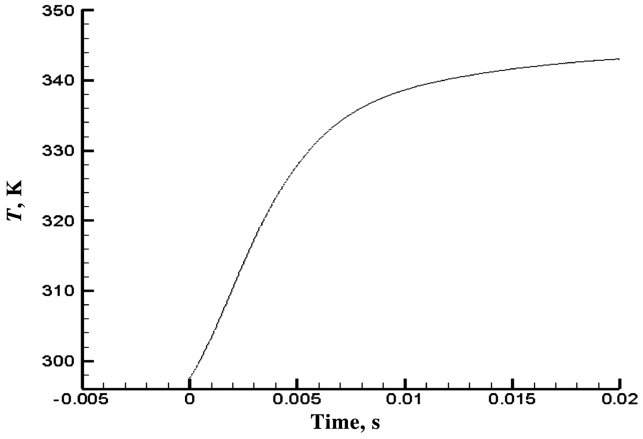

a) Early time

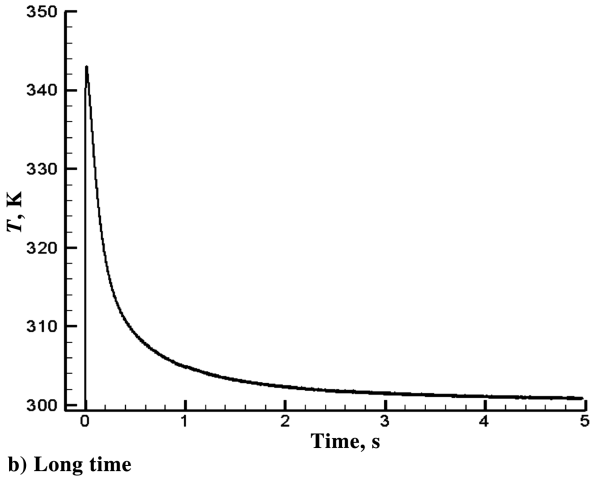

b) Long time

Fig. 5 Transient temperature of the foil; $C = 27$ mF and $V_0 = 30$ V.

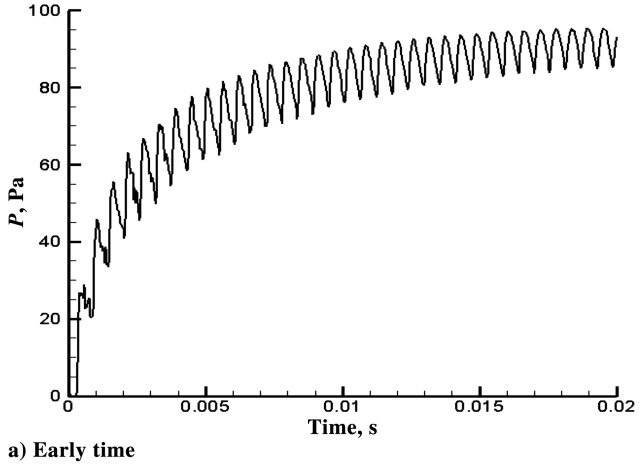

a) Early time

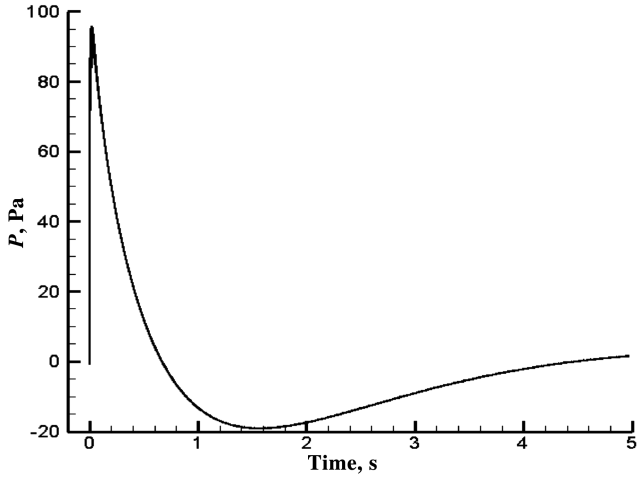

b) Long time

Fig. 6 Experimental trace of pressure ($p - p_{atm}$) variation measured by the B&K microphone; $C = 27$ mF and $V_0 = 30$ V.

$M = 1.03$. The pressure variation recorded by the Brüel & Kjær 4193 microphone over a longer period of time (about 5.1 s) is presented in Fig. 6b. It is interesting to observe that the probe records pressure values lower than the ambient value (nonphysical) beginning at about $t = 0.6$ s. The anomalous result is traced to the inherent construction and operational feature of the Brüel & Kjær condenser microphone. The existence of the narrow vent hole (see Fig. 2a) causes the nonphysical results at longer times. Although the Brüel & Kjær microphone is suitable for the measurement of the dynamic pressure (when the static pressure remains constant), it is not designed for the measurement of varying static pressure. When the foil is first heated, it heats the gas inside the tube, and so the static pressure increases. The static pressure inside the tube increases to a maximum value, then decreases to the initial value in several seconds as the heat is lost to the outside environment from the wall. Because the diameter of the vent hole connecting the microphone housing to the pressure field in the tube is very small, the static pressure inside the microphone housing varies slower than that of the pressure field in the tube. In some time periods, the static pressure inside the microphone housing becomes greater than that of the air in the tube, causing the pressure readings to fall below zero (from $t = 0.6$ to 4.2 s in Fig. 6b). Finally, the static-pressure difference between the microphone housing and the tube is eliminated (due to the cooling of the system), and the pressure measurement will be equal to the zero, as shown in Fig. 6b by $t = 5.0$ s.

A second pressure probe, the Endevco 8507C-1 piezoresistive pressure transducer, is also used in the experiments. Different from the Brüel & Kjær 4193 microphone, the vent hole of the Endevco 8507C-1 pressure transducer is exposed to the outside of the test section (see Fig. 2b), and so the variation of static pressure inside the test section does not cause any anomalous result. The unfiltered measurements are shown in Figs. 7a and 7b for the same experimental conditions described earlier for Figs. 6a and 6b. At the early time, the pressure waves measured by both probes are quite similar except that the noise generated by the Endevco probe is much higher and causes distortion in the signal. More interestingly, the two measured pressure shapes are very different for longer times (Figs. 6b and 7b), for reasons already discussed.

To decrease the noise in the Endevco probe results, the signal is digitally filtered by using the third-order Butterworth method. The comparison between the measurements by the two pressure probes (filtered results for the Endevco probe) is given in Fig. 8. No apparent negative (lower than ambient) pressure signal is found for the Endevco probe, due to its construction and measurement principle. From our experiments, we find the Brüel & Kjær microphone to be useful for the measurements of the dynamic-pressure wave (provided that there is no variation in the background static pressure), and the Endevco pressure transducer is useful for the measurement of the overall temporal pressure variations.

2. *Effects of the Capacitor Charge Voltage*

A series of measurements are carried out in which the capacitor charge voltage is varied. Figure 9 shows the effects of the charge voltage on the temporal decay of voltage across the foil for which $C = 27$ mF. The corresponding temperature measurements are given in Fig. 10. Any change of the charge voltage of the capacitor only changes the electric energy stored in the capacitor, but does not affect the characteristics of the circuit. The variation of the maximum voltage drop across the foil with the charge voltage is found to be almost linear.

Figure 11 exhibits the effects of charge voltage of the capacitor on the acoustic wave (early time) as measured by the Brüel & Kjær

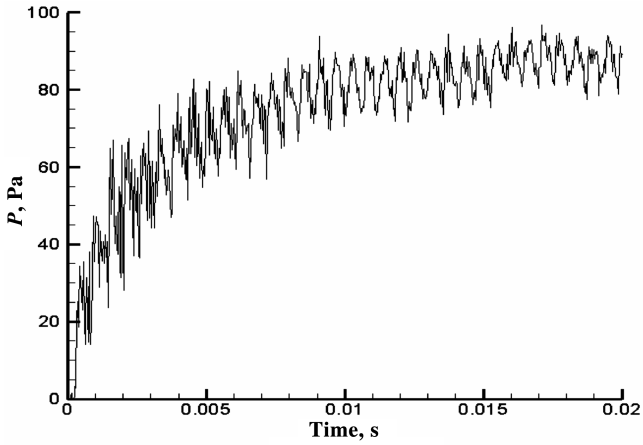

a) Early time

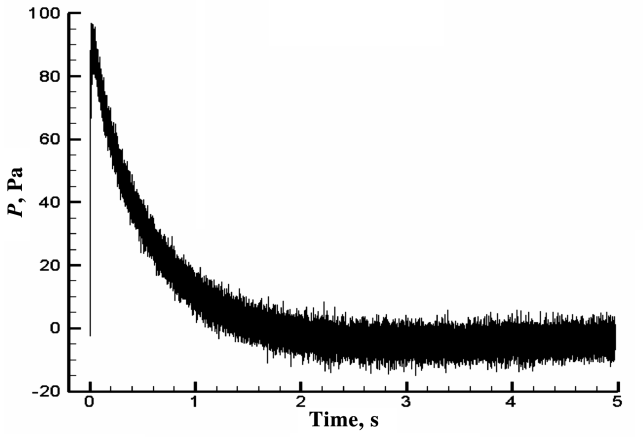

b) Long time

Fig. 7 Experimental trace of (unfiltered) pressure wave ($p - p_{atm}$) by the Endevco pressure transducer; $C = 27$ mF and $V_0 = 30$ V.

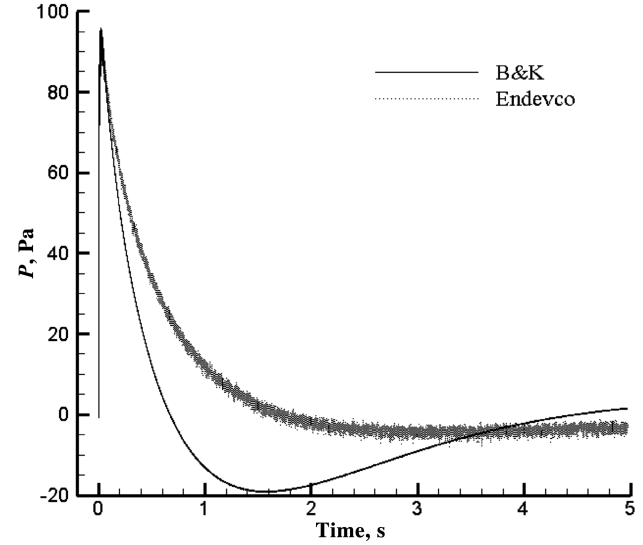

Fig. 8 Comparison of pressure ($p - p_{atm}$) measurement by the Brüel & Kjær microphone (unfiltered) and Endevco pressure transducer (filtered); $C = 27$ mF and $V_0 = 30$ V.

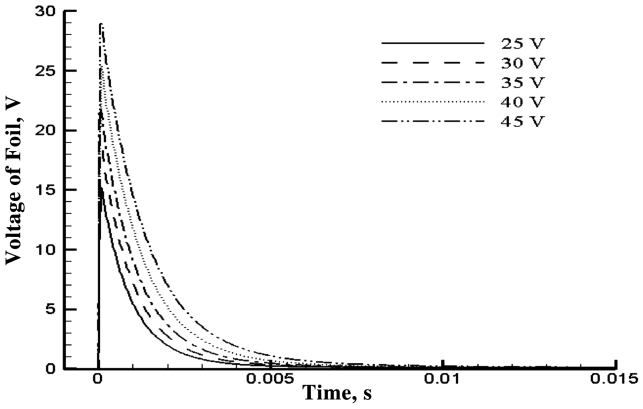

Fig. 9 Effects of the charge voltage on the temporal decay of voltage drop across the foil; $C = 27$ mF.

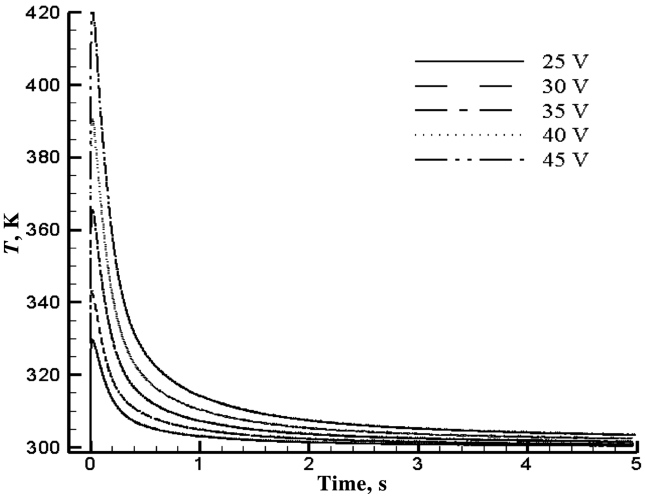

Fig. 10 Effects of the charging voltage on the (long time) temperature history of foil; $C = 27$ mF.

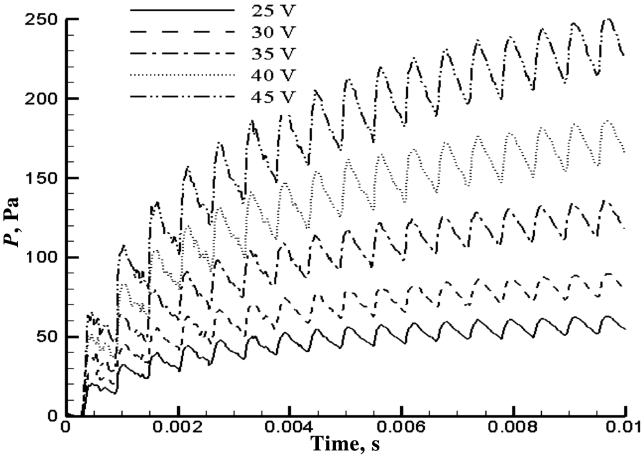

Fig. 11 Effects of the charge voltage on the pressure ($p - p_{atm}$) wave (early time) as measured by the Brüel & Kjær microphone; $C = 27$ mF.

microphone under similar conditions. Stronger acoustic waves are generated for higher charge voltages, because of the higher temperature-increase rate. Also, the static-pressure increase is higher for the higher charge voltage. Physically, the acoustic wave originates from the local pressure disturbance near the wall introduced by a sudden gas-temperature increase. The sudden gas-temperature increase is due to the heat conduction from the foil that is rapidly heated. The strength of the generated acoustic wave is found to vary almost linearly with the charge voltage.

3. *Effects of the Capacitor Value*

Figure 12 shows the effects of the capacitor value on the voltage decay rate across the foil at $V_0 = 30$ V as the capacitor is discharged.

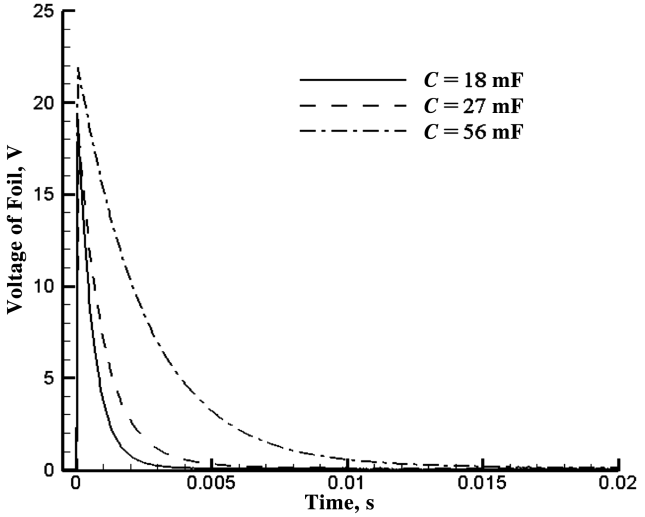

Fig. 12 Effects of the capacitance on the voltage drop across foil at early times; $V_0 = 30$ V.

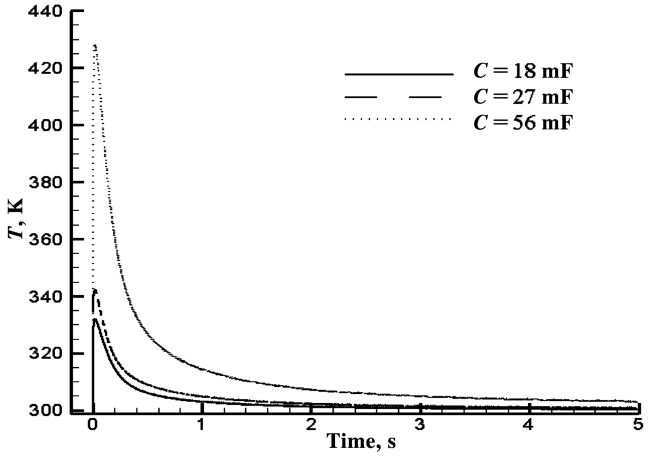

Fig. 13 Effects of the capacitance on the temperature (long time) response of the foil; $V_0 = 30$ V.

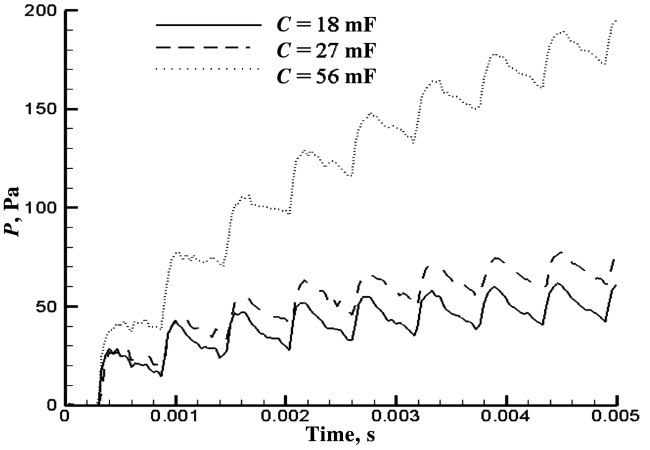

Fig. 14 Effects of the capacitance on the acoustic wave (early time) measured by the Brüel & Kjær microphones; $V_0 = 30$ V.

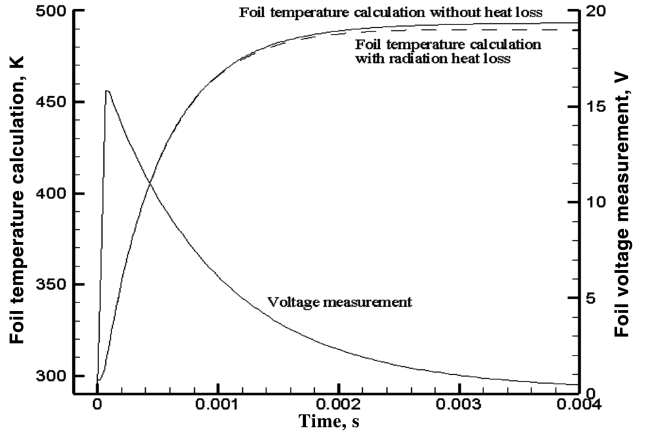

Fig. 15 Measured foil voltage and calculated foil temperature at early times; $V_0 = 30$ V and $C = 27$ mF.

The corresponding temperature measurements are given in Fig. 13. The capacitor value not only changes the amount of electric energy stored in the capacitor ($Q = CV$) but also changes the discharge character of the circuit.

Figure 14 exhibits the effects of capacitor value on the acoustic wave (early time) as measured by the Brüel & Kjær microphone under similar conditions. The higher capacitor values result in high-energy input from the foil, and so the acoustic wave generated is stronger, with higher static-pressure increases.

4. Temporal Measurements of the Foil Temperature

The experimental measurements of both voltage and temperature decay are used to develop the thermal boundary condition of the heated wall for the numerical simulations. Limited by the properties of the used thermocouple, its contact with the foil, and the electric noise of the discharging circuit, the thermocouple in our experiments cannot accurately measure the foil temperature at very early times. The foil voltage measurements and the electric energy input to the foil are used to develop the temperature decay rate at a very early time.

Figure 15 gives the foil voltage measurement and the foil temperature *calculated* from the foil voltage measurement for the case of $V_0 = 30$ V and $C = 27$ mF. In the calculation of temperature (from the voltage measurements), an energy balance equation for the foil is considered:

$$\rho c \delta A \frac{\partial T}{\partial t} = \frac{V(t)^2}{R_{\text{foil}}} + q_{\text{loss}} \tag{14}$$

where c is the specific heat of foil, A is the foil area, q_{loss} is the total heat loss of foil to the ambient environment, and $V(t)$ is voltage response of the foil. Here, we consider two kinds of cases: 1) no heat loss, $q_{\text{loss}} = 0$, and 2) heat loss by radiation, $q_{\text{loss}} = q_{\text{rad}} = \alpha\sigma_b(T_{\text{foil}} - T_{\text{ambient}})$, where α is the absorptivity of the foil (0.36) and σ_b is the Stefan–Boltzmann constant. The preceding equation is numerically solved by an explicit scheme. From the calculated temperature profiles (with and without heat loss), we find from Fig. 15 that the heat loss term has only slight effect on the foil temperature during the temperature rise time (within 0.001 s).

Figure 16 shows the comparison of the calculated foil temperature (with radiation heat loss) from the voltage measurements and the thermocouple temperature measurements. As stated earlier, the thermocouple data are conditioned by an Omega Omni Amp IIB-E conditioning amplifier. The adhesive (silver paint) used slows down the response of the thermocouple. These effects perhaps cause the measured temperature data at the early time to be underpredicted (Fig. 16). For larger values of time, somewhat different reasons (heat losses) cause the discrepancy between the measured and predicted values of the temperature. There are several sources of heat loss, such as convective heat loss to air and conduction losses to the copper bars and the mica plate, that are not considered in Eq. (14). Independent experiments in simple systems confirmed that the temperature measurements at larger values of time ($t > 0.1$ s) are accurate. A polynomial fit of the measured data is obtained for $t > 0.1$ s. We extend the polynomial fit for the measured temperature decay from

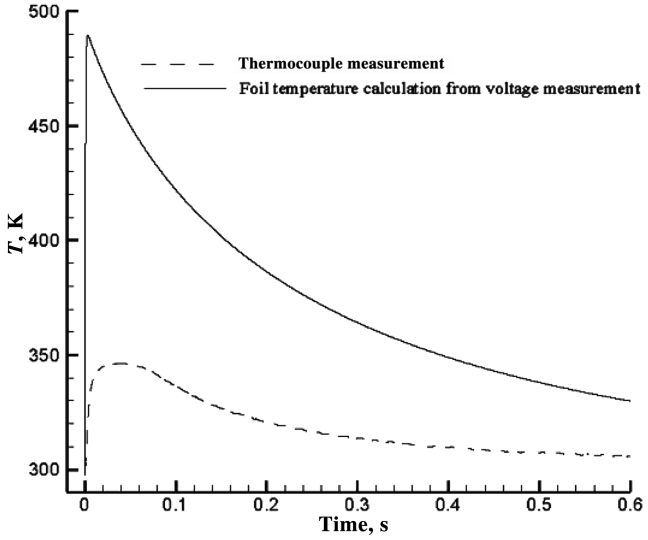

Fig. 16 Calculated foil temperature (with radiation heat loss) and thermocouple measurements; $V_0 = 30$ V and $C = 27$ mF.

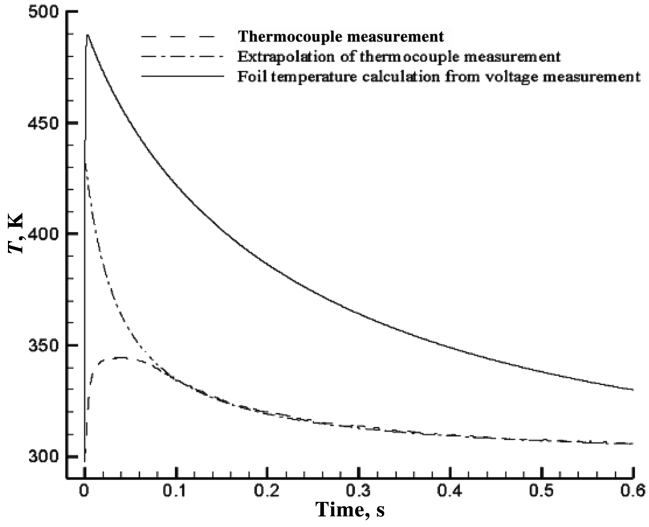

Fig. 17 Extrapolation of measured foil temperature; $V_0 = 30$ V and $C = 27$ mF.

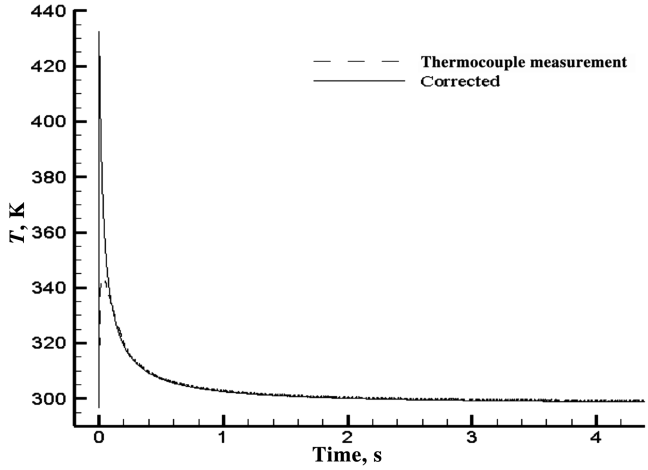

Fig. 18 Measured and calculated foil temperature history; $V_0 = 30$ V and $C = 27$ mF.

$t = 0.1$ to 0.0001 s, as shown in Fig. 17. For the experiments, the foil temperature increases rapidly and then gradually decays. The predicted temperature increase of the foil (from the voltage measurement) meets the extrapolated curve of the temperature decay at about $t = 0.0007$ s. This is close to the calculated circuit time constant $\tau_{RC} = R_{\text{total}} \cdot C = 0.00071$ s for $C = 27$ mF, as discussed earlier in Sec. II.A.

The extrapolated temperature profile for the foil (from the measured data at larger times) is shown in Fig. 18 for $0 > t > 4.4$ s. The initial temperature rise for the foil is given as follows:

When $0 > t > 0.0007$ s,

$$T = a_0 + \sum_{i=1}^{8} [a_i \times \cos(i \times 1000 \times t \times w) + b_i \times \sin(i \times 1000 \times t \times w)] + 297.636 \tag{15}$$

where $a_0 = 140.3$, $a_1 = -60.57$, $a_2 = -34.98$, $a_3 = -22.27$, $a_4 = -13.28$, $a_5 = -6.817$, $a_6 = -2.757$, $a_7 = -0.7334$, $a_8 = -0.05938$, $b_1 = -30.39$, $b_2 = -13.74$, $b_3 = -2.497$, $b_4 = 2.769$, $b_5 = 4.091$, $b_6 = 3.337$, $b_7 = 1.943$, $b_8 = 0.7773$, and $w = 2.393$. and

When 0.0007 s $> t > 4.2$ s,

$$T = \frac{a}{10t + b} + 297.636 \tag{16}$$

where $a = 50.92$ and $b = 0.3704$

The preceding corrected temperature history [Eqs. (15) and (16)] for $0 > t > 4.2$ s is used as the temperature input in our numerical simulations of the experimental case in which $V_0 = 30$ V and $C = 27$ mF. The method is used to obtain foil temperature histories for other cases with different charge voltages and capacitances.

B. Numerical Results

The generation of acoustic waves by a rapidly heated surface is simulated by numerically solving the compressible Navier–Stokes equations. The nature of the acoustic waves generated are strongly dependent on the rate of increase of the heated foil and its subsequent cooling. In the earlier section, we described the procedure we followed to develop the temporal boundary condition for the heated foil (initial rapid increase followed by gradual cooling) that we used in the numerical simulations [16].

The numerical model described earlier [16] is used to obtain the predictions of the flow and pressure fields in tube driven by rapid heating of the foil, as shown in Figs. 19a and 19b. The thermal boundary condition for the foil was given earlier: Eq. (15) for $0 > t > 0.0007$ s and Eq. (16) for 0.0007 $s > t > 4.2$ s. For the pressure at the midpoint of the tube wall, the comparison of the numerical and experimental results is given in Figs. 19a, in which $V_0 = 30$ V and $C = 27$ mF. In the first several acoustic cycles ($t < 0.002$ s), the numerical and experimental results show excellent agreement. The good agreement between the computational and experimental pressure results demonstrates that the method for considering the transient foil temperature is reasonable. The comparison of the predictions with the measurements at larger times (up to 0.03 s) is shown in Fig. 19b. In the experiments, the acoustic energy is partially absorbed by the walls when the wave hits a wall, which is not accounted for in the present simulations. In the numerical model, all walls are considered smooth and rigid. There is also a possibility of the existence of leakage in the experimental setup. The simulations are carried out with a sealed domain and also with a small opening (0.1% of the tube length) at the end (see Fig. 3). The numerical results correctly predict the pressure wave speed and amplitude of dynamics pressure fluctuation to be the same as in the experimental results. The pressure response in the computational study (for the sealed tube), however, is found to decay slower in the simulations compared with the experimental measurements. The computed pressure response decays faster for the case with the opening, as shown in Fig. 19b. Compared with the sealed case, the

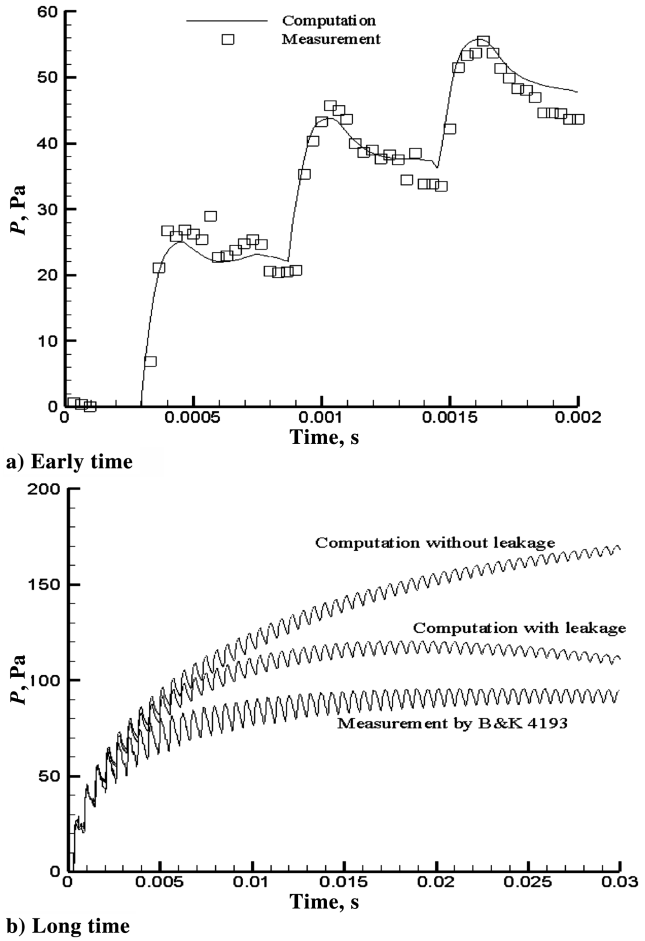

Fig. 19 Comparison of experimental and computational pressure wave profiles; $V_0 = 30$ V and $C = 27$ mF.

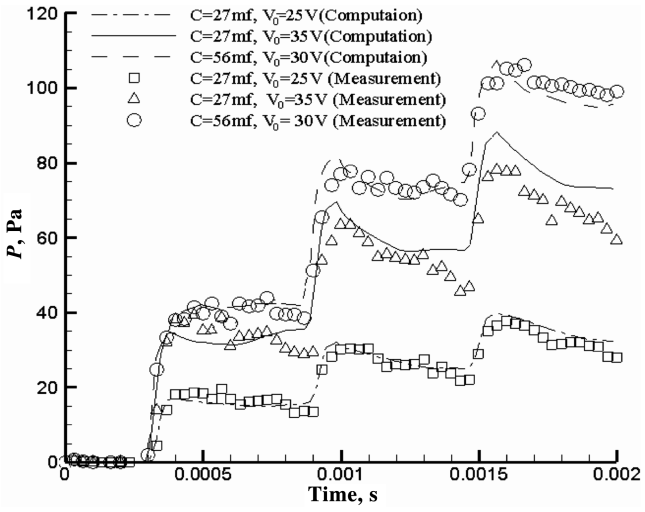

Fig. 20 Comparison of experimental and computational pressure wave profiles for different charging voltages and capacitances.

pressure response in this case is much closer to the experimental results.

Figure 20 shows the comparison of experimental data and numerical predictions of pressure (at the midpoint of tube wall) for three cases: $C = 27$ mF and $V_0 = 25$ V, $C = 27$ mF and $V_0 = 35$ V, and $C = 56$ mF and $V_0 = 30$ V. The computational and experimental results are found to have the same acoustic speeds and similar wave shapes. The maximum deviation between the experimental measurements and numerical predictions is about -7% for the case with $C = 27$ mF and $V_0 = 35$ V. The computational results are always found to slightly underpredict the results, for the reasons already explained.

C. Estimation of Experimental Uncertainty

Several independent measurements are performed for the completion of the experimental study. These measurements are the gas pressure in the tube (Brüel & Kjær 4193 microphone and Endevco 8507C-1 pressure transducer), foil temperature measured by fine thermocouple, and the measurement of voltage decay across the foil. All measurements are recorded by the NI 6052E DAQ board. The accuracy of the NI 6052E is ± 4.747 mV for the range of voltage measurements for the 4193 microphone, ± 0.479 mV for the 8507C-1 pressure transducer measurements, and ± 0.242 mV for the thermocouple measurements.

There are two sources of error in the Brüel & Kjær 4193 microphone system: ± 0.2 dB from the 4193 microphone itself and ± 0.1 dB from the 2690 signal conditioner. With the error induced by the DAQ board, the total maximum error for the pressure measurement by the Brüel & Kjær 4193 microphone is estimated to be ± 0.15 Pa. There are also two sources of error in the Endevco 8507C-1 pressure transducer system: the uncertainty of the Endevco 8507C-1 pressure transducer is 0.25% of the full-scale output (6895 Pa), and the 4428A signal conditioner is 0.2% of the full-scale-output uncertainty. The total uncertainty of the 8507C-1 pressure transducer system is ± 31.03 Pa.

The errors in the thermocouple measurement include ± 0.045°C error from the cold junction compensation, ± 0.02°C error from the conversion equation, and ± 0.08°C error from the DAQ board. The total temperature error is ± 0.145°C. The only error in the voltage measurement is from the DAQ board, which is ± 7.47 mV.

The uncertainty associated with the experimental data is estimated by using the method recommended by Kline and McClintock [17]. Both the transient pressure measurement by the Brüel & Kjær 4193 microphone and the voltage measurement exhibit very good degrees of consistency and very low uncertainties. For the 4193 microphone measurement, the uncertainty is 0.75% for the experimental case with the lowest charging voltage and capacitance. The corresponding uncertainty is 0.07% for the voltage measurement. The transient pressure measurement by the Endevco 8507C-1 pressure transducer show significant noise, due to the uncertainty being close to the amplitude of pressure fluctuation. The maximum uncertainty is $\pm 1.0\%$ for the temperature measurement.

The ambient temperature for all runs is within $\pm 0.6\%$ of 299 K, and the ambient pressure is within $\pm 1\%$ of the standard atmospheric pressure. The error associated with the variation of the ambient conditions is considered to be minor.

V. Conclusions

Experimental measurements and numerical simulations are carried out to characterize the generation, development, and decay of thermally induced acoustic waves in a cylindrical tube. In the experiments, the development and the decay of pressure waves inside the tube are investigated by two different pressure probes, and the different results are attributed to the physical construction of the two probes. The strength of acoustic waves generated is found to be linearly dependent on the temperature increase rate of the foil at early times. A numerical model based on the direct numerical simulation of the Navier–Stokes equations is developed to simulate the experiments. In the early times, the computational and experimental results are in excellent match. The experimental measurements and numerical results for the pressure evolution, however, do not match well at longer times. This is perhaps due to the presence of leaks in the chamber and damping of the wall (considered rigid in the simulations). However, the physical features of the computational and experimental results are in good agreement.

Acknowledgments

The authors gratefully acknowledge support from NASA grants NNC04AA22A and NNC04IA09I. The technical support from

Martin Alexander and Niels V. Boegholm from the Brüel & Kjær Company was most helpful.

References

[1] Trilling, L., "On Thermally Induced Sound Fields," *Journal of the Acoustical Society of America*, Vol. 27, No. 3, 1955, pp. 425–431. doi:10.1121/1.1907920

[2] Zappoli, B., Amiroudine, S., Carles, P., and Ouazzani, J., "Thermoacoustic and Buoyancy-Driven Transport in a Square Side-Heated Cavity Filled with a Near-Critical Fluid," *Journal of Fluid Mechanics*, Vol. 316, 1996, pp. 53–72. doi:10.1017/S0022112096000444

[3] Trilling, L., "On Thermally Induced Sound Fields," *Journal of the Acoustical Society of America*, Vol. 27, No. 3, 1955, pp. 425–431. doi:10.1121/1.1907920

[4] Huang, Y., and Bau, H. H., "Thermoacoustic Waves in a Confined Medium," *International Journal of Heat and Mass Transfer*, Vol. 40, No. 2, 1997, pp. 407–419. doi:10.1016/0017-9310(96)00068-3

[5] Huang, Y., and Bau, H. H., "Thermoacoustic Waves in a Semi-Infinite Medium," *International Journal of Heat and Mass Transfer*, Vol. 38, No. 8, 1995, pp. 1329–1345. doi:10.1016/0017-9310(94)00271-V

[6] Ozoe, H., Sato, N., and Churchill, S. W., "The Effect of Various Parameters on Thermoacoustic Convection," *Chemical Engineering Communications*, Vol. 5, Nos. 1–4, 1980, pp. 203–221. doi:10.1080/00986448008935964

[7] Ozoe, H., Sato, N., and Churchill, S. W., "Numerical Analyses of Two- and Three-Dimensional Thermoacoustic Convection Generated by a Transient Step in the Temperature of One Wall," *Numerical Heat Transfer, Part A, Applications*, Vol. 18, No. 1, 1990, pp. 1–15. doi:10.1080/10407789008944780

[8] Brown, M. A., and Churchill, S. W., "Finite-Difference Computation of the Wave Motion Generated in a Gas by a Rapid Increase in the Bounding Temperature," *Computers and Chemical Engineering*, Vol. 23, No. 3, 1999, pp. 357–376. doi:10.1016/S0098-1354(98)00279-8

[9] Farouk, B., Oran, E. S., and Fusegi, T., "Numerical Study of Thermoacoustic Waves in an Enclosure," *Physics of Fluids*, Vol. 12, No. 5, 2000, pp. 1052–1061. doi:10.1063/1.870360

[10] Aktas, M. K., and Farouk, B., "Numerical Simulation Of Developing Natural Convection in an Enclosure Due to Rapid Heating," *International Journal of Heat and Mass Transfer*, Vol. 46, No. 12, 2003, pp. 2253–2261. doi:10.1016/S0017-9310(02)00522-7

[11] Lin, Y., Farouk, B., and Oran, E. S., "Flows Induced by Thermoacoustic Waves in an Enclosure: Effect of Gravity," *Journal of Thermophysics and Heat Transfer*, Vol. 20, No. 3, 2006, pp. 376–383.

[12] Parang, M., and Salah-Eddine, A., "Thermoacoustic Convection Heat-Transfer Phenomenon," *AIAA Journal*, Vol. 22, No. 7, 1984, pp. 1020–1022.

[13] Brown, M. A., and Churchill, S. W., "Experimental Measurements of Pressure Waves Generated by Impulsive Heating of a Surface," *AIChE Journal*, Vol. 41, No. 2, 1995, pp. 205–213. doi:10.1002/aic.690410202

[14] Boris, J. P., Landsberg, A. M., Oran, E. S., and Gardner, J. H., "LCPFCT: A Flux-Corrected Transport Algorithm for Solving Generalized Continuity Equations," U.S. Naval Research Lab. Rept. NRL/MR/6410-93-7192, Washington, D.C., 1993.

[15] Poinsot, T. J., and Lele, S. K., "Boundary Conditions for Direct Simulations of Compressible Viscous Flows," *Journal of Computational Physics*, Vol. 101, No. 1, 1992, pp. 104–129. doi:10.1016/0021-9991(92)90046-2

[16] Lin, Y., Farouk, B., and Oran, E. S., "Flows Induced by Thermoacoustic Waves in an Enclosure: Effects of Gravity," *Journal of Thermophysics and Heat Transfer*, Vol. 20, No. 3, 2006, pp. 376–383.

[17] Kline, S. J., and McClintock, F. A., "Describing Uncertainties in Single-Sample Experiments," *Mechanical Engineering*, Vol. 75, Jan. 1953, pp. 3–8.